# Printed Carbon Resistive Strain Sensor for Structural Health Monitoring

Babatunde Falola[1], Shiwantha Gunathilake[1], Bryan Cabrera[1], David Demoz[1], Sophie Schwarz-Eise[1], Nafish Islam[1], Riadh Al-Haidari[1], Stephen Gonya[1], Nikky Pathak[2], Zebadiah Miles[2], Svetlana Bakhmatova[2], Mark D. Poliks[1]

[1] Center for Advanced Microelectronics Manufacturing (CAMM), Binghamton, NY 13902 USA

[2] GE Vernova, Niskayuna, NY 12308 USA

Email: bfalola1@binghamton.edu

## Abstract

Structural health monitoring (SHM) of large-scale engineering structures increasingly relies on flexible hybrid electronics (FHE) systems to enable conformal, lightweight, low-cost and scalable sensing solutions capable of sustained performance under repeated mechanical stress. This work presents the design, fabrication, and characterization of printed carbon-based resistive strain sensors for crack detection application. Serpentine trace test coupons were fabricated by dispensing carbon-based conductive pastes onto polyimide and PET substrates and evaluated under tensile loading and extended fatigue cycling with real-time four-wire resistance monitoring. Of ten conductive inks screened, two carbon pastes on polyimide demonstrated the most favorable balance of printability, gauge factor and resistance drift (5% for the best configurations). Extended fatigue testing to 15,000 cycles confirmed stable gauge factors of 4–5.7 with no significant degradation. Thin lamination encapsulation outperformed dielectric encapsulation in signal stability, with resistance drift as low as 1.4% compared to up to 15% for dielectric samples. Thermo-pressing post-processing further reduced baseline resistance by over 50% and improved gauge factor consistency, lowering standard deviation from 0.87 to 0.37. These results establish printed carbon resistive sensors with thin lamination and thermo-pressing as a scalable, low-cost platform for flexible structural health monitoring.

## Key words

Resistive strain sensor, Gauge factor, Flexible hybrid electronics (FHE), Structural health monitoring (SHM), Conductive Inks, Crack detection

## I. Introduction

Structural health monitoring (SHM) using flexible hybrid electronics (FHE) is an emerging approach for ensuring the reliability of structures subject to repeated mechanical loading, including wind turbine blades, aerospace components, and civil infrastructure. The conformable nature of FHE enables direct integration of strain sensors onto complex structural surfaces, facilitating real-time crack detection and early damage identification to prevent catastrophic failure and reduce maintenance costs. Resistive strain sensors represent one of the most widely adopted sensing modalities for this purpose, offering simplicity, high strain sensitivity low-cost fabrication, and broad compatibility with flexible substrates across structural, biomedical, and robotic applications. These devices operate on the piezoresistive principle, whereby mechanical deformation of a conductive sensing element produces a proportional change in electrical resistance, quantified by the gauge factor (GF):

$$\text{Guage Factor (GF)} = \frac{\left(\frac{\Delta R}{R_0}\right)}{\text{Strain (\%)}}$$

Traditional metallic foil gauges offer a GF of approximately 2, while emerging nanocomposite sensors achieve GF values exceeding 100 [1],[2]. Advances in flexible electronics and wireless communication have addressed key practical installation challenges, including conformability to curved surfaces and elimination of wired connections, making resistive strain sensors a realistic and low-cost approach for SHM of structures such as wind turbine blades [3].

Recent advancements in printed and flexible electronics have significantly expanded the applicability of resistive strain sensors. Screen-printed conductive composites, such as carbon black/silver hybrid inks, have demonstrated improved printability and high sensitivity, enabling scalable and low-cost fabrication processes [1]. Ink composition optimization plays a critical role in tuning sensor performance, where conductive filler distribution and

percolation networks influence gauge factor, repeatability, and mechanical reliability [2]-[5]. Similarly, graphene-based printed strain sensors exhibit high performance due to tunneling resistance changes and network deformation, providing enhanced sensitivity and stability compared to conventional materials [4]-[5]. Flexible substrates and fabrication techniques also strongly influence sensor characteristics [7]. Additive manufacturing approaches using silver nanoparticle–carbon composites have further enabled temperature and humidity-independent sensing performance, improving environmental stability for real applications [6].
Resistive strain sensors also play a critical role in large-scale structural monitoring applications. For example, piezoresistive sensing methods are widely used for detecting deformation and damage within fiber-reinforced composite structures of polymer wind turbine blades, where real-time strain monitoring enables early failure detection and improved reliability [8-9]. However, long-term durability is a key challenge, as substrate degradation and environmental exposure can affect sensor performance and mechanical properties [10].

Beyond resistive strain gauges, other sensing technologies are available. Capacitive sensors consume very little power but require more complex electronics and signal processing [11]. Fiber Bragg Grating (FBG) optical sensors provide very high accuracy and are immune to electromagnetic interference, but they are more expensive and can be fragile [12]. Inductive sensors can operate without direct electrical contact, but they are generally larger in size and can be affected by nearby metals [13].

In comparison, resistive strain sensors remain the most practical option because they are simple to manufacture, low cost, provide high strain sensitivity over large coverage area and can be used on many different substrates. These advantages make them well suited for structural health monitoring, wearable electronics, and biomedical applications, even though their gauge factor is often lower than some alternative sensing technologies [11]– [13].

Despite extensive work on printed strain sensors, there remains limited comparative data on commercially available carbon pastes, substrate selection, encapsulation strategies, and post-processing approaches under long-term cyclic loading. This work addresses these gaps through systematic electromechanical evaluation. Through systematic evaluation of ten ink–substrate combinations, encapsulation strategies, and thermo-pressing post-processing, this study identifies Asahi TU-10S and Micromax™ 7102 carbon pastes on polyimide as printable sensor configurations achieving gauge factors of 57 and 14.67 respectively, with thin lamination encapsulation limiting resistance drift to below 5% over 1000 cycles and stable performance sustained across 15,000 fatigue cycles, supporting their practical deployment in structural health monitoring applications.

## II. Materials and Methods

*A. Design, Materials and Fabrication Tools*

The resistive strain gauge test coupon is designed in AutoCAD 2025 for electrical and mechanical testing of printed piezoresistive traces. Figure 1a shows a serpentine trace with a defined active gauge length of 33.0 mm and a trace width of approximately 1.0 mm, where the folded parallel-line geometry maximizes the effective sensing length within a compact footprint to enhance piezoresistive strain sensitivity.

The fabrication of test coupons was performed using a Nordson dispensing system under optimized printing conditions, with a print speed of 10 mm/s, pressure range of 45-65psi and a 27-gauge dispensing needle. Selected conductive pastes were deposited on Kapton and PET substrates for subsequent electrical, adhesion, and mechanical performance evaluation. Each paste–substrate combination was thermally cured or sintered according to the recommended processing conditions.

*B. Electromechanical Evaluation*

The printed samples were mechanically tested using an MTS Acumen electrodynamic testing machine, with resistance measured in real time using a Keithley DAQ 6510 data acquisition system. Four-wire resistance measurements were recorded at a sampling rate of 10 readings per second throughout all tests. For monotonic testing, strain was applied in 0.5% increments up to a maximum of 3% (see Fig. 1c), with each increment applied over a 1-second ramp followed by a 60-second dwell period before proceeding to the next increment. The samples were then unloaded back to 0% strain using the same incremental steps. For fatigue testing, samples were cycled between 0% and 3% strain for 1000 cycles at a frequency of 1 Hz.

## III. Results and Discussion

The screening of ten conductive inks (see **Table 1**) was carried out based on three primary criteria: print quality (print edge resolution and adhesion), electrical behavior (resistance drift), and mechanical durability (guage factor).

*A. Stretching Test*

A uniaxial stretching test was conducted to evaluate the gauge factor (GF) and signal drift of the fabricated strain sensors. The test included one loading and unloading cycle. The samples were strained from 0% to 3% in 0.5% increments. A 1-minute rest was applied at each step. The samples were then unloaded back to 0% strain at the same rate. Resistance drift was evaluated to quantify signal stability over repeated loading (See Table 2). Drift was calculated by comparing the baseline resistance at 0% strain before cycling ($R_{0,initial}$) and after completion of 1000 cycles ($R_{0,final}$): Drift (%) $= \frac{R_{0,final} - R_{0,initial}}{R_{0,initial}} \times 100$

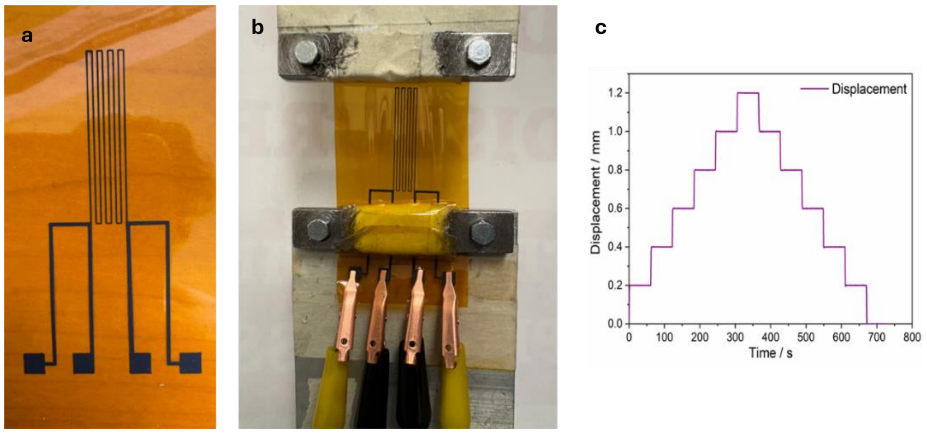



**Figure 1 (a–c):** (a) Test coupon design on PI substrate, (b) sample mounted on the MTS Acumen testing system, and (c) displacement profile of the monotonic stretching test.

Table 1: Materials summary of evaluated conductive inks and substrate materials.

| # | Ink | Ink Volume Resistivity | Description | Substrates |
|---|---|---|---|---|
| 1 | **Asahi TU-10S CARBON PASTE** | < 10 Ω/square/mil | Flexible Carbon paste. Consists of carbon and graphite powder | PI/PET |
| 2 | **ACI FC3203** | < 10 Ω/square/mil | Flexible Carbon paste | PI/PET |
| 3 | **Micromax™ 7102** | 20-30 Ω/square/mil | Flexible Carbon paste | PI/PET |
| 4 | **Micromax® PE671** | 500 Ω/square/mil | Stretchable Carbon paste | PI/PET/TPU |
| 5 | **C250J Carbon Paste** | 8 Ω/square/mil | Flexible Carbon paste | PI/PET |
| 6 | **DOWA nanoparticle silver ink** | 1-2 mΩ/square/mil | AgNP | PI/PET |
| 7 | **AGFA Nanosilver Ink SI-P2000** | 2 mΩ/square/mil | AgNP | PI/PET |
| 8 | **Micromax™ 5025** | 8-15 mΩ/square/mil | Flexible Ag paste. Consists of Ag Microflakes | PI/PET/TPU |
| 9 | **Mixture of Micromax™ 5025 And Micromax™ 7102** | NA | C (80%): Ag (20%) | PI/PET |
| 10 | **Mixture of Micromax™ 5025 And Micromax™ 7102** | NA | C (60%): Ag (40%) | PI/PET |

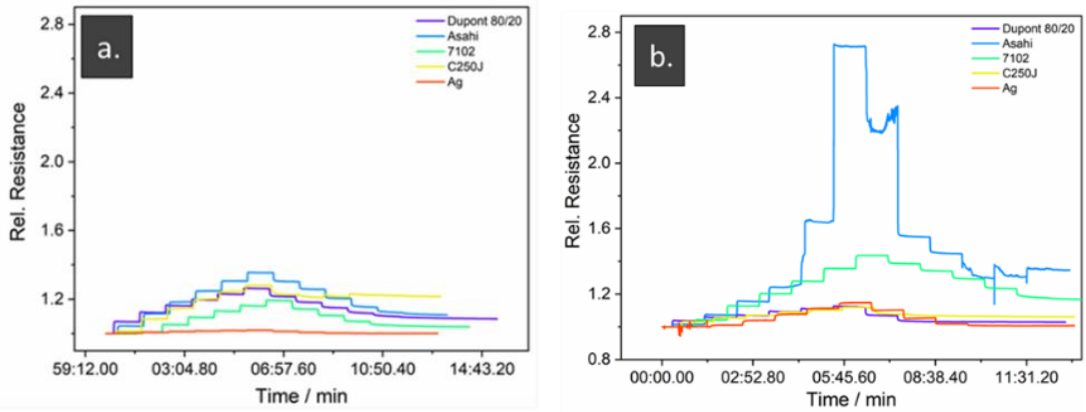



**Figure 2 (a–b):** Change in relative resistance versus time (displacement) for the tested inks on (a) PET and (b) PI substrates.

The high performing inks are highlighted in **Table 2**. These include Asahi TU-10S carbon paste on PET and PI substrates, Micromax™ 7102 carbon paste, and mixtures of Micromax™ 5025 and Micromax™ 7102 at two different ratios on PI substrate. Among all the inks tested, Agfa silver ink on PI shows the lowest initial resistance. Also, this ink exhibits the highest gauge factors. However, non-uniformity and higher resistance drift after 1000 cycles of fatigue testing make this ink less appealing to consider further as a resistive sensor candidate ink.

*B. Fatigue Cycling*

Fatigue testing was conducted to evaluate the electromechanical stability of the strain sensors under repeated deformation. The samples were subjected to cyclic uniaxial tensile strain of 3% at a frequency of 1 Hz for 1000 cycles using MTS Acumen testing machine. Electrical resistance was recorded continuously during the cycling test using a Keithley DAQ 6510 data acquisition system.

The fatigue cycling results (see **Table 3**) suggest that the Asahi carbon on PI has the highest gauge factor and high resistance drift. Asahi carbon paste on PET shows the lower resistance drift, but the gauge factor is also lower relative to the Asahi on PI. Asahi carbon paste on PI shows more balanced performance. It achieves a high gauge factor with relatively low resistance drift. A similar performance was observed with Micromax™ 7102 carbon paste.

Table 2: Resistance drift and gauge factor of different inks on PET and PI substrates after initial stretch test (green boxes are the selected material)

| Substrate | Ink | Initial R (Ω) | Gauge Factor | R Drift (%) |
|---|---|---|---|---|
| PI | Dupont 80/20 | 7051 | 4.1 | 2.8 |
| PET | Dupont 80/20 | 3549 | 8.72 | 8.6 |
| **PI** | **Asahi C** | 3366 | **57** | 34.7 |
| **PET** | **Asahi C** | 2154 | 11.82 | 10.8 |
| PI | C250J | 28418 | 3.97 | 6.1 |
| PET | C250J | 37905 | 9.37 | 21.6 |
| **PI** | **7102 C** | 44137 | 14.67 | 15.9 |
| PET | 7102 C | 37345 | 6.37 | 3.9 |
| PET | Agfa Ag NP. | 26.3 | 4.87 | 0.6 |
| PET | Agfa Ag NP. | 9.6 | 0.63 | 0.1 |
| PET | DOWA NP. Ag | 3 | broken | broken |
| PI | DOWA NP. Ag | 3.72 | broken | broken |

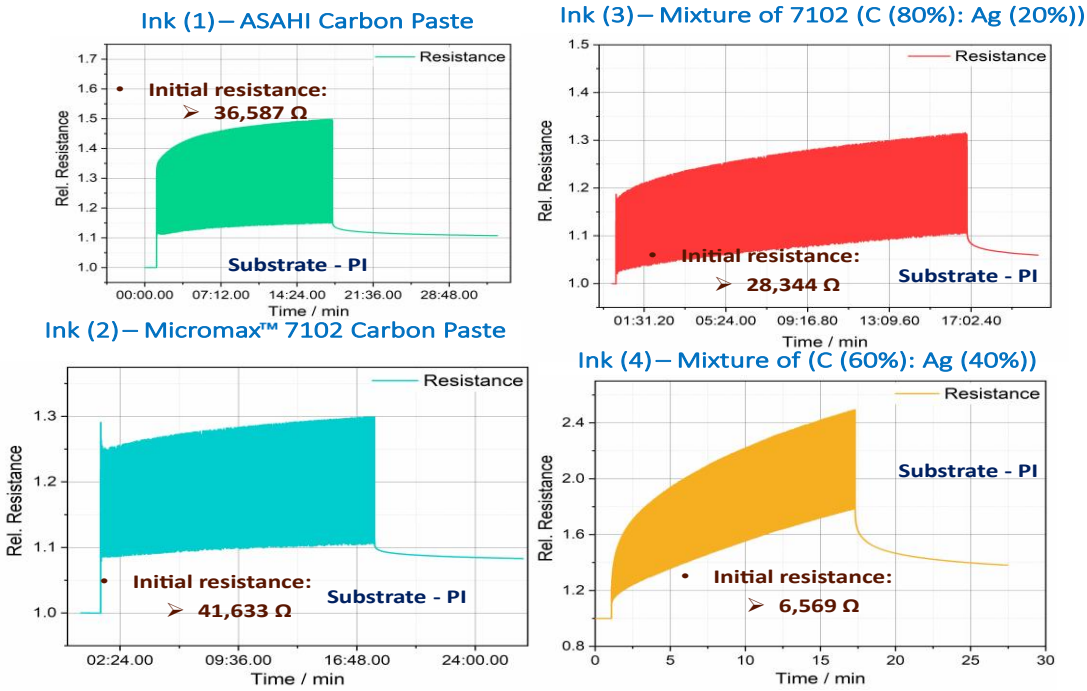



Figure 3: Fatigue cycling results for the four downselected inks on PI

Table 3: Resistance drift and gauge factor for 2nd, 500th, and 1000th cycles after fatigue cycling – ignoring the 1st cycle.

| Substrate | Ink | Initial R / Ω | GF 1st cycle | GF – 2nd Cycle | GF 500th cycle | GF 1000th cycle | R Drift (%) 1st cycle | R Drift (%) 2nd cycle |
|---|---|---|---|---|---|---|---|---|
| PI | C:Ag (80:20) | 38,002 | 6.2 | 5 | 6.1 | 6.0 | 6 | 3.3 |
| PI | C:Ag (80:20) | 28,344 | 9.9 | 5.3 | 6.2 | 6.4 | 16.3 | 5 |
| **PI** | **Asahi C** | **36,587** | **9.7** | **7.8** | **13.9** | **15.6** | **9.4** | **3.9** |
| **PI** | **Asahi C** | **46,331** | **10.2** | **6.8** | **9.6** | **9.8** | **10.7** | **0.36** |
| **PET** | **Asahi C** | **20,700** | **8.7** | **4.1** | **4.4** | **6.5** | **6.7** | **-5.1** |
| **PI** | **7102 C** | **32,625** | **10.2** | **5.5** | **6.0** | **6.0** | **9.5** | **0.18** |
| **PI** | **7102 C** | **41,633** | **9.7** | **5.8** | **5.4** | **5.8** | **8.3** | **4.9** |
| PI | C:Ag (60:40) | 6,210 | 5.4 | 2.9 | 9.7 | 9.3 | 36 | 26.8 |
| PI | C:Ag (60:40) | 6,569 | 7.6 | 4.8 | 14.1 | 12.9 | 38.2 | 22.9 |

### C. *Effect of first-cycle resistance jump on Gauge Factor and Drift*

It was observed that during the first loading–unloading cycle, the sensors exhibited a noticeable resistance jump, resulting in an apparent variation in the calculated gauge factor and an increase in baseline drift. This behavior is commonly attributed to initial microstructural rearrangement within the conductive network, such as filler realignment, microcrack stabilization, or contact resistance adjustment under mechanical loading [14].

The first-cycle response is attributed to a conditioning or stabilization process rather than steady-state sensing behavior. The gauge factor and resistance drift were therefore recalculated excluding the first cycle, with baseline resistance redefined at the start of the second cycle, yielding substantially more stable gauge factors and lower resistance drift, as summarized in **Table 3**.

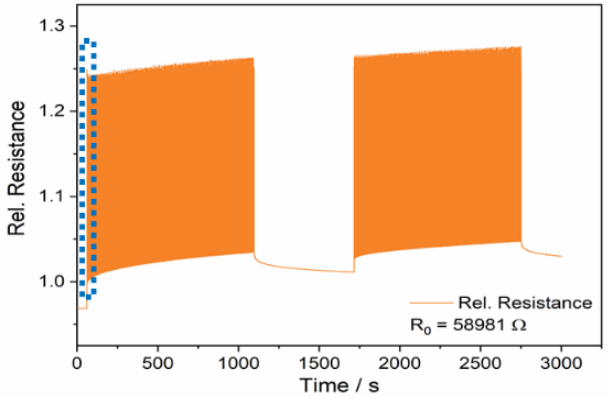



Figure 4: The variation of resistance with the number of cycles, with 10 minutes rest between fatigue cycles

To investigate whether the initial resistance jump was a one-time conditioning effect or an inherent response of the material system, an additional experiment was conducted. After completing 1000 fatigue cycles at 3% strain and 1 Hz, the samples were allowed to rest for 10 minutes under zero strain. Subsequently, another set of 1000 fatigue cycles were applied under identical conditions.

The results indicate that the resistance jump reappeared during the first loading cycle of the second test sequence. This confirms that the phenomenon is not limited to the initial test but occurs each time cyclic loading is reinitiated after a rest period. The repeated first-cycle resistance increase suggests reversible microstructural relaxation during the rest interval, followed by rapid reconfiguration of the conductive network upon reloading.

It was further observed that the gauge factor became progressively more stable as the cycle number increased (see **Tables 3-4**). Figure 4 illustrates the two fatigue cycles conducted after 10 minutes of rest.

### D. *Effect of Encapsulation and Lamination*

Based on the promising performance in earlier testing, two resistive carbon-based inks (Asahi TU-10S and Micromax™ 7102) were selected for sensor evaluation. Resistive strain gauges were fabricated on PI and two selected encapsulation materials (Dupont 5036 and Dupont ME778) were applied as shown in Figure 5 (a-b) to evaluate sensor performance and material compatibility. The effect of the lamination was also investigated using two different lamination materials from Covestro [Thin laminate (MA5000) and thick laminate (D-2539-19)] as shown in Figure 5 (c-d) respectively.

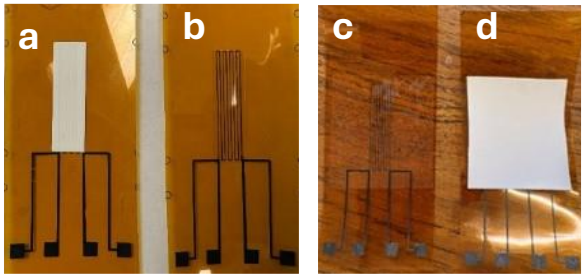



Figure 5 (a-d): Image of the (a-b) resistive sensors encapsulated with ME778 and Dupont 5036 encapsulation materials. (c-d) thin and thick laminate materials on the printed sensor

The summarized results from this test are given in **Table 5**, and the study showed that the thin laminated sensor with Asahi carbon paste configuration exhibits the lowest variation in gauge factor compared to all tested samples, followed by the same lamination with Micromax 7102 ink. This also suggests that minimizing the additional material layers above the sensing element improves strain transfer while reducing unwanted changes in electrical behavior. The findings also indicate that the encapsulation materials may interact with the printed carbon sensing layer, influencing overall sensor performance. Possible interactions include partial penetration of the encapsulation material into the porous printed carbon network, surface wetting effects, or mechanical constraint introduced during curing or lamination. These effects can alter the conductive pathways within the carbon trace, leading to changes in baseline resistance, increased drift, or reduced signal stability during cyclic loading [14]-[18].

The results showed that the strain sensors maintained a generally stable gauge factor throughout the 15,000-cycle evaluation, demonstrating good long-term electromechanical reliability (see Fig. 7). While slight variations in gauge factors were observed between individual test segments and across different days, the overall response remained consistent, with no significant degradation in sensing performance. Tables 6, 7 and 8 demonstrate the calculated gauge factors for each day. Within each day of testing, the gauge factor remained relatively stable across successive cycle intervals, indicating that the sensor retained repeatable strain sensitivity even after extended cyclic loading.

The small variations observed between test sessions may be attributed to several factors. These include minor differences in how the sensor was mounted or aligned in the mechanical test fixture, which can affect strain transfer to the sensing element, as well as microstructural evolution within the printed conductive network during repeated deformation, such as gradual rearrangement of conductive pathways. In addition, hysteresis and viscoelastic relaxation in the substrate or laminated sensor structure may contribute to small shifts in baseline response after resting periods. Despite these effects, the overall stability of the gauge factor across 15,000 cycles indicates strong durability and supports the suitability of the printed strain sensor for long-term cyclic sensing applications.

Table 4: Table of values for gauge factor and drift for 2nd, 500th, and 1000th cycles for sensor fabricated with 7102 Carbon paste

| Steps | GF 2nd Cycle | GF 500th cycle | GF 1000th cycle | Resistance Drift (%) |
|---|---|---|---|---|
| 1 | 8.2 | 6.9 | 6.9 | **1.1** |
| 2 | 7.8 | 6.8 | 6.3 | **1.2** |

Table 6: Calculated gauge factors for day 1

| Cycle | 2nd | 1k | 2k | 3k | 4k | 5k | 6k | 7k | 8k | 9k | 10k |
|---|---|---|---|---|---|---|---|---|---|---|---|
| GF | 2.6 | 3.5 | 3.7 | 3.8 | 3.8 | 3.9 | 3.9 | 4 | 4 | 4 | 4 |

Table 7: Calculated gauge factors for day 2

| | GF: 2nd Cycle | GF: 500th cycle | GF: 1000th cycle |
|---|---|---|---|
| 1 | 5.0 | 4.9 | 5.0 |
| 2 | 5.4 | 5.2 | 5.2 |

Table 8: Calculated gauge factors for day 3

| | GF: 2nd Cycle | GF: 500th cycle | GF: 1000th cycle |
|---|---|---|---|
| 1 | 5.7 | 5.6 | 5.5 |
| 2 | 5.9 | 5.6 | 5.6 |
| 3 | 5.7 | 5.7 | 5.7 |

Table 5: Comparison of GF with different encapsulation methods

| Ink | | Asahi TU-10S CARBON PASTE | | | | Micromax™ 7102 | | | |
|---|---|---|---|---|---|---|---|---|---|
| Encapsulation | 1000 cycles | GF – 2nd Cy. | GF – 500th Cy. | GF – 1000th Cy. | Resistance Drift (%) | GF – 2nd Cy. | GF – 500th Cy. | GF – 1000th Cy. | Resistance Drift (%) |
| TPU Laminated | 1 | 6.7 | 6.1 | 5.9 | 2.2 | 4.2 | 2.4 | 2.3 | 5.8 |
| | 2 | 6.7 | 5.9 | 5.8 | 1.4 | 3 | 2.3 | 2.2 | 1.3 |
| Printed Dupont 5036 | 1 | 5.8 | 4.7 | 4.8 | 6.1 | 3.3 | 2.2 | 2.6 | 7.8 |
| | 2 | 5.2 | 4.4 | 4 | 1.3 | 2.8 | 2.6 | 2.1 | 1.7 |
| Printed ME778 | 1 | 3.9 | 1.8 | 1.7 | 15 | 1.11 | 2.68 | 2.4 | 10.3 |
| | 2 | 2.3 | 1.7 | 1.7 | 3.1 | 0.95 | 2.33 | 2.2 | 3.1 |
| Baseline | 1 | 6.8 | 9.6 | 9.8 | 0.36 | 8.2 | 6.9 | 6.9 | 1.1 |
| | 2 | 7.8 | 6.8 | 6.3 | 1.2 | 7.8 | 6.8 | 6.3 | 1.2 |

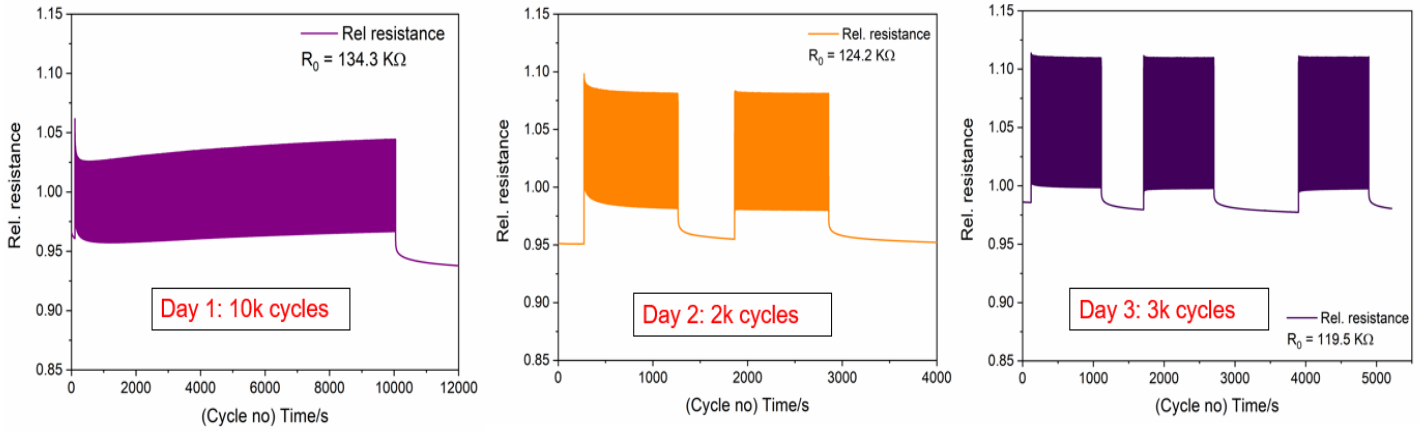



Figure 6: 15,000 cycles at 1 Hz rate profile across 3 days

*E. Adhesion Test*

The crosshatch adhesion test was conducted for the two high performing pastes Asahi and 7102 carbon on both PET and PI substates and the ASTM rating shows acceptable performance.

**Table 9:** Cross-cut adhesion test results (ASTM D3359) for selected carbon-based inks on PET and PI substrates.

| Inks/Substrates | PET | PI |
|---|---|---|
| Asahi TU- 10S | 4B | 3B |
| Micromax™ 7102 | 5B | 4B |

*F. Effect of Thermo-pressing*

Strain sensors fabricated with additional heat pressing step were also tested to investigate the long-term fatigue cycling performance. For this test, the strain gauge printed using Micromax 7102 and thin lamination was used. Samples were heat pressed at 165℃ for 10 minutes at 100 psi pressure. Samples were tested for 15,000 fatigue cycles across day 1 and day 2 using same cycling loading profile. The goal was to determine whether heat pressing could improve the consistency and durability of the printed carbon sensing layer under repeated strain. Figure 7 shows the testing profiles across two days.

The results showed that heat pressing reduced the initial resistance of the printed carbon traces by more than 50% compared with non-heat-pressed samples [14],[19]. This reduction suggests improved densification and consolidation of the printed carbon network, likely caused by enhanced particle-to-particle contact and reduced porosity within the conductive layer. The applied heat and pressure may also improve adhesion between the printed ink and PI substrate, creating a more uniform conductive path and lowering contact resistance throughout the sensor.

In addition to the reduction in baseline resistance, the heat-pressed sensors exhibited more stable gauge factor behavior during fatigue cycling. Compared with untreated samples, which had a standard deviation of 0.87 for the gauge factor, the heat-pressed sample only showed a standard deviation of 0.37. **Table 8** shows the comparison of gauge factors between heat-pressed and non-heat-pressed samples. This improved stability indicates that heat pressing help stabilize the conductive microstructure, reducing rearrangement of conductive pathways during repeated deformation.

Overall, the results suggest that heat pressing is a beneficial post-processing method for printed carbon strain sensors, improving both electrical conductivity and long-term sensing stability under cyclic mechanical loading.

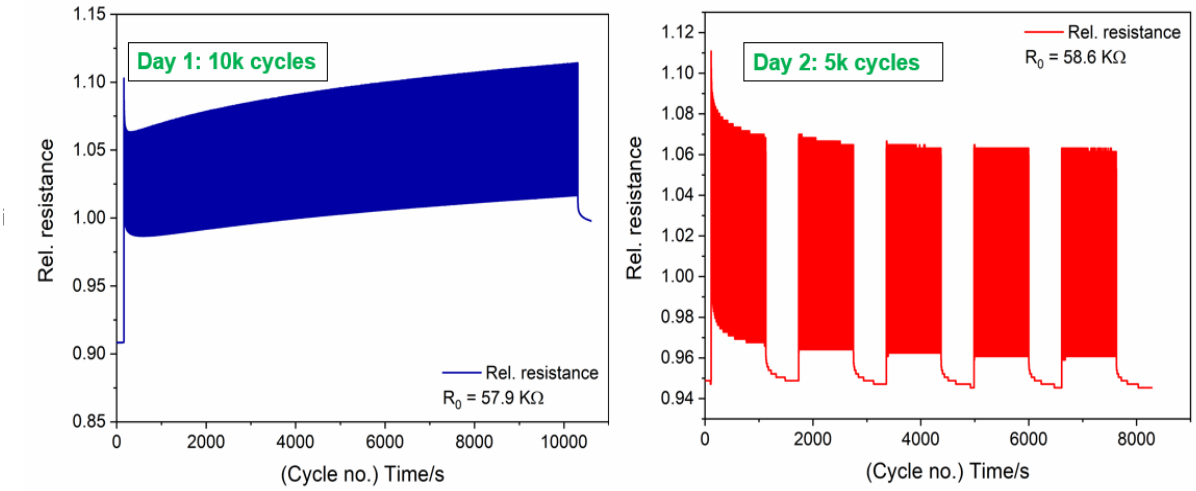



Figure 7: Fatigue cycling profiles for two days. Day 1 - 10,000 cycles and Day 2 - 5,000 cycles with 10 min. rest after each 1,000 cycles

## IV. Conclusion

This work demonstrated the design, fabrication, and electromechanical characterization of dispense printed carbon-based resistive strain sensors for flexible crack detection applications. Of the ten conductive inks screened, Asahi TU-10S and Micromax™ 7102 carbon pastes on polyimide substrates exhibited the most favorable balance of printability (adhesion rating 4B), gauge factor and resistance drift, achieving gauge factors of 57 and 14.67 respectively during initial stretching tests, with corresponding resistance drift values of 34.7% and 15.9%. A reversible first-cycle resistance transient, attributed to initial conditioning of the conductive network, was observed across the tested inks; excluding this transient reduced resistance drift substantially (e.g., from 9.4% to 3.9% for Asahi C on PI, and from 16.3% to 5% for the C80/Ag20 mixture), yielding more stable gauge factor and drift metrics. Extended fatigue testing to 15,000 cycles across three days confirmed that the sensors retained a stable gauge factor (ranging from approximately 4 to 5.7 across the test sequence) with no significant long-term degradation, supporting their viability for sustained cyclic loading.

Encapsulation strategy was found to strongly influence sensor performance: thin TPU lamination preserved gauge factor stability more effectively than dielectric encapsulation, with the Asahi TU-10S/thin-laminate configuration showing the lowest variation in gauge factor (5.8–6.7) and drift as low as 1.4% after 1000 cycles, compared to gauge factors as low as 1.7–3.9 and drift up to 15% for the ME778-encapsulated samples. Thermo-pressing of the printed Micromax™ 7102 carbon traces further reduced baseline resistance by more than 50% and improved

gauge factor consistency, lowering the standard deviation in gauge factor from 0.87 (untreated) to 0.37 (heat-pressed). These results establish printed carbon-based resistive sensors, particularly Asahi TU-10S carbon and Micromax™ 7102 carbon on polyimide with thin lamination and thermo-pressing, as a scalable, low-cost option for flexible structural health monitoring.

## Future Work

Future work will focus on extending reliability testing beyond 15,000 fatigue cycles to further validate long-term electromechanical stability under sustained cyclic loading conditions. Process-level optimization will be pursued to improve print consistency, trace uniformity, and adhesion across large-area. Additional investigation will explore the effect of environmental factors, including temperature, humidity, and mechanical bending, on sensor performance and encapsulation integrity. The integration of wireless sensing capabilities and multiplexed sensor arrays will also be examined to support practical deployment in structural health monitoring systems.

## Acknowledgment

The authors would like to thank NextFlex for sponsoring this research with funds from the Air Force Research Laboratory under Agreement Number FA8650-20-2-5506**.** The U.S. Government is authorized to reproduce and distribute reprints for governmental purposes, notwithstanding any copyright notation thereon. The views and conclusions contained herein are those of the authors and should not be interpreted as necessarily representing the official policies or endorsements, either expressed or implied, of Air Force Research Laboratory, the Air Force Research Laboratory, or the U.S. Government.

## References

[1] X. Qi, H. Ha, B. Hwang, and S. Lim, “Printability of the Screen-Printed Strain Sensor with Carbon Black/Silver Paste for Sensitive Wearable Electronics,” Applied Sciences 2020, Vol. 10, Page 6983, vol. 10, no. 19, p. 6983, Oct. 2020, doi: 10.3390/APP10196983.

[2] Mahmoud, H. A., Nesser, H., Mostafa, T. M., Ahmed, S., & Lubineau, G. (2025). A Fully Printable Strain Sensor Enabling Highly-Sensitive Wireless Near-Field Interrogation. *Advanced science (Weinheim, Baden-Wurttemberg, Germany)*, *12*(9), e2411346. https://doi.org/10.1002/advs.202411346

[3] N. Anderson, N. Szorc, V. Gunasekaran, S. Joshi, and G. Jursich, “Highly sensitive screen-printed strain sensors on flexible substrates via ink composition optimization,” Sens Actuators A Phys, vol. 290, pp. 1–7, May 2019, doi: 10.1016/J.SNA.2019.02.028.

[4] Z. Zhou, W. Tang, T. Xu, W. Zhao, J. Zhang, and C. Bai, “Flexible Strain Sensors Based on Thermoplastic Polyurethane Fabricated by Electrospinning: A Review,” Sensors (Basel), vol. 24, no. 15, p. 4793, Aug. 2024, doi: 10.3390/S24154793.

[5] E. Caffrey, J. R. Garcia, D. O’Suilleabhain, C. Gabbett, T. Carey, and J. N. Coleman, “Quantifying the Piezoresistive Mechanism in High-Performance Printed Graphene Strain Sensors,” ACS Appl Mater Interfaces, vol. 14, no. 5, p. 7141, Feb. 2022, doi: 10.1021/ACSAMI.1C21623.

[6] C. Sánchez, D. Rodríguez, S. Otero, and C. A. Monje, “Enhancing sensing performance of 3D-printed TPU/CB piezoresistive strain sensors through integration of silver ink IDE,” Sens Actuators A Phys, vol. 393, p. 116757, Oct. 2025, doi: 10.1016/J.SNA.2025.116757.

[7] [6] I. Nadeem et al., “Fabrication of Temperature- and Humidity-Independent Silver Nanoparticle’s Carbon Composite-Based Strain Sensor Through Additive Manufacturing Process,” 3D Print Addit Manuf, vol. 10, no. 4, p. 674, Aug. 2023, doi: 10.1089/3DP.2021.0032.

[8] H. Kang, S. Kim, J. Shin, and S. Ko, “Inkjet-Printed Flexible Strain-Gauge Sensor on Polymer Substrate: Topographical Analysis of Sensitivity,” Applied Sciences 2022, Vol. 12, Page 3193, vol. 12, no. 6, p. 3193, Mar. 2022, doi: 10.3390/APP12063193.

[9] W. Wang, Y. Xue, C. He, and Y. Zhao, “Review of the Typical Damage and Damage-Detection Methods of Large Wind Turbine Blades,” Energies 2022, Vol. 15, Page 5672, vol. 15, no. 15, p. 5672, Aug. 2022, doi: 10.3390/EN15155672.

[10] S. Nauman, “Piezoresistive Sensing Approaches for Structural Health Monitoring of Polymer Composites—A Review,” Eng 2021, Vol. 2, Pages 197-226, vol. 2, no. 2, pp. 197–226, May 2021, doi: 10.3390/ENG2020013.

[11] M. Vasylius, A. Tadžijevas, D. Šapalas, V. Kartašovas, J. Janutėnienė, and P. Mažeika, “Degradation of Mechanical Properties of A-PET Films after UV Aging,” Polymers 2023, Vol. 15, Page 4166, vol. 15, no. 20, p. 4166, Oct. 2023, doi: 10.3390/POLYM15204166.

[12] Z. Zhang et al., "Liquid Metal Interdigitated Capacitive Strain Sensor with Normal Stress Insensitivity," *Adv. Intell. Syst.*, vol. 4, no. 4, p. 2100201, Apr. 2022, doi: 10.1002/aisy.202100201.

[13] Alhussein et al. “Fiber Bragg Grating Sensors: Design, Applications, and Comparison with Other Sensing Technologies” Sensors (Basel). 2025 Apr 4;25(7):2289. doi: 10.3390/s25072289. PMID: 40218802; PMCID: PMC11991054.

[14] A. Masi, M. Falchi, D. Brizi, E. Canicattì, G. Nenna, and A. Monorchio, "Inductive Frequency-Coded Sensor for Non-Destructive Structural Strain Monitoring of Composite Materials," Sensors, vol. 24, no. 20, p. 6725, Oct. 2024, doi: 10.3390/s24206725.

[15] B. Falola et al., "Evaluation of Materials for the Design and Development of Sustainable Low-Cost Single-Use Electrode Leads for Wearable Medical Devices," 2024 IEEE 74th Electronic Components and Technology Conference (ECTC), Denver, CO, USA, 2024, pp. 179-186, doi: 10.1109/ECTC51529.2024.00038.

[16] Shamsian, Olya Noruz, Babatunde Falola, Abdullah Obeidat, Riadh Al-Haidari, Jordan Howard-Jennings, Bryan Cabrera, Udara Somarathna, et al. 2025. “Eco-Friendly, High-Performance Cellulose Acetate Encapsulation for Flexible Hybrid Electronics: Environmental Stability and Printing Scalability.” *IMAPSource Proceedings* 2025 (Symposium): 350–55. https://doi.org/10.4071/001c.147221.

[17] B. Falola, O. N. Shamsian, R. Al-Haidari, U. Somarathna, B. Cabrera, M. Alhendi, M. D. Poliks, G. S. Khinda, T.-J. Kao, N. Stoffel, and R. Tudela, "Printed Vertical Interconnect Accesses Enhanced Circuits on Flexible Substrates: Process Optimization and Evaluation," in *SMTA International 2025*, vol. 27, no. 1, pp. 36–42, Oct. 2025, doi: 10.37665/smMDHIJ95992.

[18] S. Lieberman et al., "Electrical Behavior of Thin Die Assembly on Flexible Substrate Under Vibration Testing," 2024 IEEE 74th Electronic Components and Technology Conference (ECTC), Denver, CO, USA, 2024, pp. 1670-1676, doi: 10.1109/ECTC51529.2024.00276.

[19] B. Falola, R. Al-Haidari, O. N. Shamsian, S. Gunathilake and M. D. Poliks, "Thermo-Pressing Treatment to Enhance Conductivity of Printed Carbon on Flexible Substrates," 2026 IEEE 76th Electronic Components and Technology Conference (ECTC), Orlando, FL, USA, 2026, pp. 2330-2337, doi: 10.1109/ECTC51846.2026.00386.